https://doi.org/10.5194/acp-2019-1011
Preprint. Discussion started: 2 December 2019

Atmospheric Chemistry and Physics Discussions

Integrated impacts of synoptic forcing and aerosol radiative effect on boundary layer and pollution in the Beijing-Tianjin-Hebei region, China

Yucong Miao[1], Huizheng Che[1], Xiaoye Zhang[1], Shuhua Liu[2]

[1]State Key Laboratory of Severe Weather & Key Laboratory of Atmospheric Chemistry of CMA, Chinese Academy of Meteorological Sciences, Beijing 100081, China
[2]Department of Atmospheric and Oceanic Sciences, School of Physics, Peking University, Beijing 100871, China

Correspondence to: H. Che (chehz@cma.gov.cn) and X. Zhang (xiaoye@cma.gov.cn)

Abstract. Rapid urbanization and industrialization have led to deterioration of air quality in the Beijing-Tianjin-Hebei (BTH) region with high loadings of $PM_{2.5}$. The heavy aerosol pollutions frequently occur in winter, closely in relation to the meteorological conditions. To unravel the complicated impacts of large-scale atmospheric forcing and the local-scale planetary boundary layer (PBL) characteristics on the pollution there, this study combined long-term observational data analyses, synoptic pattern classification, and meteorology-chemistry coupled simulations. During the winter of 2017 and 2018, Beijing, Langfang, Tianjin, and Tangshan often simultaneously experienced heavy $PM_{2.5}$ pollution, accompanying with strong thermal inversion aloft. These concurrences of pollution in different cities were primarily regulated by the large-scale atmospheric processes. Using the principal component analysis with the geopotential height fields at the 850-hPa level during winter, the typical polluted synoptic pattern in BTH was identified. The pattern was featured by westerly winds from upstream mountainous regions. By inducing warm advections from the west, the thermal inversion aloft in the BTH could be enhanced, leading to shallow daytime PBLs and high near-surface $PM_{2.5}$ concentrations. In addition, the aerosol may also modulate the PBL structure through its radiative effect, which was examined using numerical simulations. The aerosol radiative effect can significantly lower the boundary layer height in the afternoon through cooling the surface layer and heating the upper part of PBL. Thus, more aerosols could be accumulated in the lower portion of PBL, bringing about heavy pollution in the BTH. This study has revealed the important roles played by the meteorology-aerosol interaction on the air quality.

1 Introduction

The Beijing-Tianjin-Hebei (BTH) region is the national capital region of China, and covers an area of ~217,156 km^2 in the North China Plain. During the last few decades, the BTH has experienced prosperous economic growth and intensive urban expansion, and becomes one of most developed and populous regions in China. Along with the tremendous development, pollution events with massive $PM_{2.5}$ (airborne particles with aerodynamic diameter less than 2.5 μm) frequently occur in the BTH, due primarily to the high emissions (Cheng et al., 2016; Geng et al., 2017; Zhang et al., 2013).

https://doi.org/10.5194/acp-2019-1011
Preprint. Discussion started: 2 December 2019

Atmospheric Chemistry and Physics Discussions

The fate of emitted pollutants is largely governed by the planetary boundary layer (PBL) (Garratt, 1994; Miao and Liu, 2019; Oke, 2002; Stull, 1988), which is the region of the lower troposphere and strongly influenced by the surface. The PBL acts as changeable coupling agents that modulate momentum, heat, moister, and matter between the surface and free troposphere (Baklanov et al., 2011; Miao et al., 2019a; Stull, 1988). In the vertical dimension, the intensity of thermal buoyancy is controlled by the thermal stratification, and the strength of mechanical turbulence is determined by the surface roughness and the PBL wind. Together these thermal and mechanical PBL processes determine the vertical dispersion and dilution of pollutants and the air replacing from upper levels (Miao et al., 2019a; Oke, 2002; Stull, 1988). Thereby, the depth of PBL, also known as the boundary layer height (BLH), has been extensively utilized to characterize the atmospheric environmental capacity and the dilution volume of pollutants (Stull, 1988; Seidel et al., 2010; Hu et al., 2014; Miao et al., 2015).

Through observational experiments and numerical simulations, the associations between the PBL characteristics and aerosol pollution in the BTH have been investigated (e.g., Miao et al., 2019b; Quan et al., 2013; Wang et al., 2018a; Ye et al., 2016; Zhong et al., 2017, 2018). The heavy $PM_{2.5}$ pollution events in BTH typically occur under stagnant situations with shallow PBL (Ye et al., 2016; Zhong et al., 2017 and 2018). On a seasonal basis, the heaviest aerosol pollution in BTH occurs in winter, which is not only ascribed to the seasonal changes in emissions and precipitation, but also the shifts in the BLH (Miao et al., 2015, 2018b). With mountains and seas surrounded (Fig. 1), the PBL process/structure and pollution level in the BTH are usually impacted by the geographical forcings (Chen et al., 2009; Hu et al., 2014, 2016, Miao et al., 2015, 2016, 2017b). Due to the blocking effects of mountains, the momentum exchanging processes between the PBL and the upper free troposphere could be repressed dynamically (Miao et al., 2018; Wang et al., 2018b). Moreover, the local thermal gradient between the mountains-and-plains or land-and-sea can bring on closed circulation systems, and modify the near-surface winds and thermal inversion intensity, leading to the re-circulation and accumulation of pollutants (Chen et al., 2009; Miao et al., 2015, 2017b, 2019a).

In addition to these local-scale surface factors/processes (e.g., friction, thermally induced wind systems, heat fluxes), the large-scale synoptic pattern (e.g., transient systems, thermal advections) plays a role in supplying the foremost driving for the day-to-day variations of BLH and pollution (Hu et al., 2014; Miao et al., 2019b; Stull, 1988). Although the previous studies have recognized the importance of PBL characteristics for the aerosol pollution in the BTH, most of them focused on the processes in a specific city (e.g., Miao et al., 2019b; Quan et al., 2013; Tie et al., 2015; Wang et al., 2019; Zhong et al., 2017). More investigations are warranted concerning (1) the unfavorable PBL characteristics of heavy pollution concurring in several cities of BTH, and (2) the relevant synoptic conditions. These aspects are yet to be clearly known, partly due to the absence of continuous PBL observations in the different major cities in the BTH. In this study, the PBL-aerosol associations in the BTH will be examined using the long-term radiosonde measurements collected in Beijing and Tangshan (Fig. 1b): one close to the mountains and the other adjacent to the Bohai Sea.

On the other hand, during the heavy pollution events, the black carbon can cause the upper layer of PBL to be relatively warm (Ding et al., 2016), and the massive aerosols can intensify the PBL stability through scattering the solar radiations, leading to lower the BLH and deteriorate the pollution (Miao et al., 2019a; Quan et al., 2013; Sun et al., 2019; Wang et al., 2019; Zhong

https://doi.org/10.5194/acp-2019-1011
Preprint. Discussion started: 2 December 2019

Atmospheric Chemistry and Physics Discussions

et al., 2017, 2018). For instance, the unfavorable PBL meteorology and the feedback of aerosol together, were found to be responsible for ~84% of the explosive growth of $PM_{2.5}$ concentration in Beijing during December 2016 (Zhong et al., 2017). Considering that the large-scale synoptic forcing is the first-order meteorological driving for the pollution formation/dissipation, it would be necessary to examine the impacts of aerosol radiative effect on BLH on the basis of synoptic pattern analyses. Thus, this study will objectively classify the synoptic patterns over the BTH during winter from 2017 to 2018, and then evaluate the integrated impacts of aerosol radiative effect on PBL structure under typical synoptic condition using the meteorology-chemistry coupled simulations. The combination of large-scale synoptic analyses and numerical simulations allows us to understand the complicated meteorology-aerosol interaction in the BTH within an integrated framework.

2 Data and Methods

The aerosol pollution levels in BTH are indicated by the hourly measurements of $PM_{2.5}$ mass concentration from 2017 to 2018 in four major cities, including Beijing, Langfang, Tianjin, and Tangshan (Fig. 1b). For each studied city, there are three $PM_{2.5}$ monitoring sites (illustrated by red crosses in Fig. 1b) carried out by the China National Environmental Monitoring Center (CNEMC). Besides, the radiosonde measurements in Beijing and Tangshan were collected to elucidate the complex associations between the PBL meteorology and aerosol pollution. The sounding stations (illustrated by green triangle in Fig. 1b) are equipped with the L-band radiosonde system (Miao and Liu, 2019), which can provide the vertical profiles of pressure, moisture, air temperature, and wind with a fine resolution (~10 m). The sounding balloons are conventionally launched at 0800 and 2000 Beijing Time (BJT) during a day. In addition, the surface meteorological observations (illustrated by black dots in Fig. 1b) were also obtained in all the studied cities.

To unravel the predominant synoptic conditions related to the heavy aerosol pollution in the BTH, the 850-hPa geopotential height (GH) fields were analyzed, which were extracted from the National Centers for Environmental Prediction (NCEP) global Final (FNL) reanalysis. Using the T-mode principal component analysis (T-PCA) (Huth, 1996; Miao et al., 2017a; Philipp et al., 2014), the dominant synoptic patterns in the BTH were objectively classified. The T-PCA has been widely to analyze the regional air pollutions from the synoptic perspective, and demonstrated to be a dependable approach to ravel out the influences of large-scale atmospheric forcing (e.g., Miao et al., 2017a; Stefan et al., 2010; Zhang et al., 2012). In consideration of the heavy $PM_{2.5}$ pollution events primarily occurred during winter (Miao et al., 2018), the daily GH fields in the winter months (January, February, November, December) of 2017 and 2018 were classified in this study.

After identifying the typical polluted synoptic pattern, two pollution episodes (EP1 and EP2 in Fig. 2) in December 2017 were selected and simulated using the Weather Research and Forecasting model coupled with Chemistry (WRF-Chem) (Grell et al., 2005). The WRF-Chem simulations were designed to understand how the large-scale synoptic forcings impact the PBL characteristics and to what extent the aerosol radiative effect influences the BLH and pollution level.

In the WRF-Chem simulations, two one-way nested domains with horizontal resolutions of 33 km and 6.6 km were used (Fig. 1a), and the inner domain covered the whole BTH (Fig. 1b). The model top was set to the 10-hPa level, and 48 vertical layers

https://doi.org/10.5194/acp-2019-1011
Preprint. Discussion started: 2 December 2019

Atmospheric Chemistry and Physics Discussions

were configured below the top. To resolve the PBL structure, 21 vertical layers were set below 2 km above ground level (AGL). For the simulation of chemistry processes, the CBMZ mechanism and MOSAIC aerosol scheme (Zaveri, 1999; Zaveri et al., 2008) were used with the Multi-resolution Emission Inventory for China (MEIC) of 2016, which is the most updated and extensively utilized anthropogenic emission data. The physics parameterization schemes used in this work included the NOAH land surface scheme (Chen and Dudhia, 2001), the Mellor-Yamada PBL scheme (Nakanishi and Niino, 2006), the WRF Single-Moment-5-class (WSM5) scheme (Hong et al., 2004), the Betts-Miller-Janjic cumulus scheme (Janjić, 1994), and the updated rapid radiation scheme considering the aerosol radiative effect (Iacono et al., 2008). The initial and boundary conditions (IBCs) of meteorological parameters were configured using the NCEP-FNL reanalysis, and the IBCs of chemical variables were derived from the global model output (http://www.acom.ucar.edu/wrf-chem/mozart.shtml).

The simulations used abovementioned configurations are referred to as the BASE runs, and numerical experiments that turned off the aerosol radiative option were conducted to evaluate the impacts of aerosol radiative effect. These sensitivity experiments are regarded as the EXP runs hereunder. According to the common strategy for the Air Quality Model Evaluation International Initiative (AQMEII), the selected pollution episodes were simulated as a sequence of three-day time slices (Forkel et al., 2015). The first 24-h simulations of each time slice were considered as the spin-up period, and the chemical initial state of each time slice is adopted from the final state of the previous time slice.

3 Results and Discussion

3.1 Linkages between synoptic condition, thermal stability and $PM_{2.5}$ pollution

The time series of daily $PM_{2.5}$ concentrations from 1 November to 31 December in 2017 are shown in Figs. 2a and 2c, demonstrating several heavy pollution episodes in the BTH. It is worth noting that all the studied cities often experienced heavy pollution simultaneously. Comparing with the observed potential temperature (PT) profiles in Beijing and Tangshan (Figs. 2b and 2d), it is clear that the quick increase (decrease) of $PM_{2.5}$ concentrations usually accompanied with the warming (cooling) of atmosphere above 1000 m AGL. Such a phenomenon not only occurred from November to December in 2017, but also other winter months during 2017 and 2018 (Figs. S1-S3). Given that the long distance between Beijing and Tangshan (~200 km), the synchronous change of aerosol concentrations in all the four cities, and the concurrence of strong thermal inversion aloft, must be relevant to certain large-scale synoptic patterns (Miao et al., 2018). Therefore, it would be necessary to investigate the $PM_{2.5}$ pollution and its influencing factors from the point of view of the large-scale conditions.

Based on the 850-hPa daily GH fields in winter from 2017 to 2018, the synoptic conditions were classified using the T-PCA (Fig. 3). There are two dominant synoptic patterns – the type 1 and type 2, which accounts for ~70% of the total. The synoptic type 1 occurs most frequently (39.6%). There is a strong southwest-to-northeast pressure gradient across the BTH, supporting to strong northwesterly prevailing winds at the 850-hPa level (Fig. 3a). For the synoptic type 2, with high pressure system to the southeast of BTH and low pressure system to the north, it is the westerly winds dominated over the BTH (Fig. 3b). The

https://doi.org/10.5194/acp-2019-1011
Preprint. Discussion started: 2 December 2019

Atmospheric Chemistry and Physics Discussions

occurrence frequency of type 2 is 30%, ranking second among all the identified synoptic types. Except for these two dominant types, the occurrence rate of other synoptic type is no more than 12.5%.

Fig. 4a exhibits the averaged $PM_{2.5}$ concentrations of each identified synoptic type in all the studied cities. Distinct difference could be found between the type 1 and type 2. The averaged $PM_{2.5}$ concentrations of type 1 are less than 62 μg m^{-3}, while type 2 is associated with heavier pollution with averaged concentrations greater than 92 μg m^{-3}. Based on the observed PT profiles, the thermal stability of each pattern were estimated as the difference between the PT values at 100 m and 1000 m AGL (Fig. 3b). Comparing with the synoptic type 1, stronger thermal stabilities are observed under the type 2 in both Beijing and Tangshan. Thus, among all the identified patterns, the synoptic type 2 can be regarded as the representative polluted pattern in the BTH, due to its high occurrence frequency, high $PM_{2.5}$ concentration, and strong thermal stability.

3.2 Typical polluted synoptic pattern and PBL structure

To unravel the complicated processes leading to the heavy pollution under the synoptic type 2, two pollution episodes in 2017 were selected and simulated using the WRF-Chem model, which were the EP1 (November 30 to December 5) and the EP2 (December 26 to 31). Fig. 5 presents the vertical structure of simulated PT in Beijing and Tangshan during those selected episodes. Comparing with the observed PT profiles shown in Figs. 2b and 2d, the warmings of atmosphere aloft during December 1-2 and December 28-29 in Beijing and Tangshan were well simulated. Furthermore, the changes of wind profile during those episodes were also accurately simulated (Fig. S4), with correlation coefficients greater than 0.73 for both the zonal and meridional winds. In Fig. 6, the simulated near-surface temperature, relative humidity, and $PM_{2.5}$ concentration are validated against the observations in all the four studied cities. Although discrepancies exist, the simulated temperature, humidity, and $PM_{2.5}$ all demonstrate rationally good agreement with the observations. These good performances of WRF-Chem (Figs. 5-6 and S4) provide a solid basis to utilize the model data to elucidate the physical mechanisms underlying the heavy pollution.

Based on the model output, the BLH is estimated as the height where the PT first surpasses the minimum PT below by 1.5 K (Nielsen-Gammon et al., 2008; Seidel et al., 2010). The same BLH derivation method has been widely employed in previous PBL studies (e.g., Hu et al., 2014; Miao and Liu, 2019; Nielsen-Gammon et al., 2008), which can explicitly manifest the influences of thermal stability. As the estimated BLH shown in Fig. 5, it is clear that the strengthening of thermal inversion suppresses the daytime BLH, and favors the accumulation of pollutants. During the EP1, the warming processes of atmosphere above PBL on December 1-2 was associated with the synoptic type 2 (Fig. 7a). Influencing by the westerly winds, the warmer air mass over the western mountainous regions could be brought to the BTH (Figs. 7c and 8a). Such a warm advection enhanced the thermal stability and restrained the growth of PBL in the BTH (Figs. 8a and 9a), resulting to high $PM_{2.5}$ concentrations at the ground-level (Figs. 8c and 9c). For example, on December 2 the daytime BLH was suppressed to less than 500 m in both Beijing and Tangshan (Fig. 5). By contrast, the daytime PBL could reach a height greater than 1500 m on December 3-4 under the synoptic type 1 (Figs. 5 and 7b). On December 3-4, the induced northwesterly cold advection not only facilitated the horizontal dispersion of pollutants, but also weakened the thermal inversion and favored the development of PBL in the BTH

https://doi.org/10.5194/acp-2019-1011
Preprint. Discussion started: 2 December 2019

Atmospheric Chemistry and Physics Discussions

(Figs. 7d, 8b, and 9b), leading to relatively good air quality there (Figs. 8d and 9d). Similar evolutions of synoptic situation and PBL structures could also be noted during the EP2. On December 28-29, the synoptic type 2 induced strong thermal inversions, shallow PBLs and high $PM_{2.5}$ concentrations in the BTH, while on December 30-31 the appearance of type 1 led to the dissipation of the pollutants (Figs. 10, S5 and S6).

3.3 Impact of aerosol radiative effect on the PBL structure and pollution

In addition to the large-scale warm/cold advections, the suspended aerosols may also modify the PBL structure to some extent (Miao et al., 2019a; Zhong et al., 2018). As shown in Fig. 11, during the EP1 the aerosol radiative effect can impose significant negative perturbations on the BLH, and positive perturbations on the ground-level aerosol concentration. By averaging over the simulation results in the region of interest (ROI) shown in Fig 11, the time series of BLH and induced perturbations of $PM_{2.5}$ and PT were derived. During the most polluted day (December 2) of the EP1, the aerosol radiative effect can lower the BLH up to 160 m in the afternoon (Fig. 12a) through cooling the surface layer below 300 m AGL and heating the upper atmosphere (Fig. 12c). Consequently, more aerosols can be accumulated in the lower portion of PBL, which can increase the ground-level $PM_{2.5}$ concentration by 28 μg m^{-3} (15%) (Fig. 12b). Similar influences of the aerosol radiative effect on the PBL and aerosol pollution could also be observed during the EP2 (Fig. S7 and S8), which can lower the daytime BLH by 110 m and increase the $PM_{2.5}$ concentration by 18 μg m^{-3} (10%). These simulation results indicate that under unfavorable synoptic condition the aerosol radiative effect plays a crucial role in enhancing the thermal stability within the PBL and exacerbating the pollution, which cannot be neglected.

4 Conclusions

To understand the critical roles of large-scale atmospheric forcing and local-scale PBL structure on the aerosol pollution in the BTH, this study combined long-term observational data analyses, synoptic classification, and meteorology-chemistry coupled simulations. On the basis of the wintertime $PM_{2.5}$ measurements and radiosonde data in four major cities (i.e., Beijing, Langfang, Tianjin, and Tangshan) from 2017 to 2018, the relationships between thermal inversion and aerosol pollution were examined. It was found that all the studied cities in the BTH often experienced high $PM_{2.5}$ concentrations simultaneously, which typically accompanied with strong thermal inversion aloft. These concurrences of heavy pollution in different cities were regulated by the large-scale synoptic forcings.

Using the T-PCA with the 850-hPa daily GH fields during winter, the typical synoptic pattern relevant to the heavy pollution in the BTH was identified. With high pressure system to the southeast of BTH and low pressure system to the north, the identified pattern is featured by the 850-hPa westerly winds over the BTH. And the warmer air mass from the western mountains could be brought to the BTH, leading to enhance the thermal inversion aloft and suppress the development of daytime PBL over the plains. Comparing with the clean situations, the induced large-scale warm advections can decrease the daytime BLH by several hundred meters, resulting to a high concentration of pollutants in the whole BTH.

https://doi.org/10.5194/acp-2019-1011
Preprint. Discussion started: 2 December 2019

Atmospheric Chemistry and Physics Discussions

In addition to the large-scale warm advections, the aerosols suspended in the atmosphere may also modulate the PBL structure. Two pollution episodes associated with the typical synoptic pattern were selected and simulated using the WRF-Chem by turning on and off the aerosol radiative option. The simulation results indicated that the aerosol radiative effect can significantly lower the BLH in the afternoon through cooling the surface layer and heating the upper part of PBL. Thereupon, more aerosols could be accumulated in the lower portion of PBL. Such a PBL-aerosol feedback mechanism plays a critical role in the explosive growth of aerosol concentration under unfavorable synoptic conditions, which should not be overlooked. Besides, although this study highlights the important roles of multi-scale physical processes in the aerosol pollution in the BTH, the chemical mechanisms/processes also should not be deemphasized.

Data availability. The reanalysis data can be downloaded from http://rda.ucar.edu/datasets/ds083.2/. The meteorological data in the BTH are available from the China Meteorological Administration (http://data.cma.cn/), and the $PM_{2.5}$ data can be obtained from the CNEMC (http://www.cnemc.cn/). The model data are available by request (chehz@cma.gov.cn).

Author contributions. Development of the ideas and concepts behind this work was performed by all the authors. Model execution, data analysis, and paper preparation were performed by YM and HC with feedback and advice from XZ and SL.

Competing interests. The authors declare that they have no conflict of interest.

Acknowledgements. This study received financial support from National Natural Science Foundation of China (41705002, 41825011), Beijing Natural Science Foundation (8192054), and Atmospheric Pollution Control of the Prime Minister (DQGG0106). The authors would like to acknowledge the Tsinghua University for the support of emission data.

References

Baklanov, A. A., Grisogono, B., Bornstein, R., Mahrt, L., Zilitinkevich, S. S., Taylor, P., Larsen, S. E., Rotach, M. W. and Fernando, H. J. S.: The nature, theory, and modeling of atmospheric planetary boundary layers, Bull. Am. Meteorol. Soc., 92(2), 123–128, doi:10.1175/2010BAMS2797.1, 2011.

Chen, F. and Dudhia, J.: Coupling an Advanced Land Surface–Hydrology Model with the Penn State–NCAR MM5 Modeling System. Part I: Model Implementation and Sensitivity, Mon. Weather Rev., 129(4), 569–585, doi:10.1175/1520-0493(2001)129<0587:CAALSH>2.0.CO;2, 2001.

Chen, Y., Zhao, C., Zhang, Q., Deng, Z., Huang, M. and Ma, X.: Aircraft study of Mountain Chimney effect of Beijing, China, J. Geophys. Res. Atmos., 114(8), 1–10, doi:10.1029/2008JD010610, 2009.

https://doi.org/10.5194/acp-2019-1011
Preprint. Discussion started: 2 December 2019

Atmospheric Chemistry and Physics Discussions

Cheng, Z., Luo, L., Wang, S., Wang, Y., Sharma, S., Shimadera, H., Wang, X., Bressi, M., de Miranda, R. M., Jiang, J., Zhou, W., Fajardo, O., Yan, N. and Hao, J.: Status and characteristics of ambient PM2.5 pollution in global megacities, Environ. Int., 89–90, 212–221, doi:10.1016/j.envint.2016.02.003, 2016.

Ding, A. J., Huang, X., Nie, W., Sun, J. N., Kerminen, V.-M., Petäjä, T., Su, H., Cheng, Y. F., Yang, X.-Q., Wang, M. H., Chi, X. G., Wang, J. P., Virkkula, A., Guo, W. D., Yuan, J., Wang, S. Y., Zhang, R. J., Wu, Y. F., Song, Y., Zhu, T., Zilitinkevich, S., Kulmala, M. and Fu, C. B.: Black carbon enhances haze pollution in megacities in China, Geophys. Res. Lett., 43, 1–7, doi:10.1002/2016GL067745, 2016.

Forkel, R., Balzarini, A., Baró, R., Bianconi, R., Curci, G., Jiménez-Guerrero, P., Hirtl, M., Honzak, L., Lorenz, C., Im, U., Pérez, J. L., Pirovano, G., San José, R., Tuccella, P., Werhahn, J. and Žabkar, R.: Analysis of the WRF-Chem contributions to AQMEII phase2 with respect to aerosol radiative feedbacks on meteorology and pollutant distributions, Atmos. Environ., 115, 630–645, doi:10.1016/j.atmosenv.2014.10.056, 2015.

Garratt, J.: Review: the atmospheric boundary layer, Earth-Science Rev., 37, 89–134, doi:10.1016/0012-8252(94)90026-4, 1994.

Geng, G., Zhang, Q., Tong, D., Li, M., Zheng, Y., Wang, S., and He, K.: Chemical composition of ambient PM2. 5 over China and relationship to precursor emissions during 2005–2012, Atmos. Chem. Phys., 17, 9187–9203, https://doi.org/10.5194/acp-17-9187-2017, 2017.

Grell, G. A., Peckham, S. E., Schmitz, R., McKeen, S. A., Frost, G., Skamarock, W. C. and Eder, B.: Fully coupled "online" chemistry within the WRF model, Atmos. Environ., 39(37), 6957–6975, doi:10.1016/j.atmosenv.2005.04.027, 2005.

Hong, S.-Y., Dudhia, J. and Chen, S.-H.: A Revised Approach to Ice Microphysical Processes for the Bulk Parameterization of Clouds and Precipitation, Mon. Weather Rev., 132(1), 103–120, doi:10.1175/1520-0493(2004)132<0103:ARATIM>2.0.CO;2, 2004.

Hu, X.-M., Ma, Z., Lin, W., Zhang, H., Hu, J., Wang, Y., Xu, X., Fuentes, J. D. and Xue, M.: Impact of the Loess Plateau on the atmospheric boundary layer structure and air quality in the North China Plain: A case study, Sci. Total Environ., 499, 228–237, doi:10.1016/j.scitotenv.2014.08.053, 2014.

Hu, X. M., Li, X., Xue, M., Wu, D. and Fuentes, J. D.: The Formation of Barrier Winds East of the Loess Plateau and Their Effects on Dispersion Conditions in the North China Plains, Boundary-Layer Meteorol., 1–19, doi:10.1007/s10546-016-0159-4, 2016.

Huth, R.: An intercomparision of computer-assited circulation classificaiton methods , Int. J. Climatol., 16(8), 893–922, doi:10.1002/(SICI)1097-0088(199608)16:8<893::AID-JOC51>3.0.CO;2-Q, 1996.

Iacono, M. J., Delamere, J. S., Mlawer, E. J., Shephard, M. W., Clough, S. A. and Collins, W. D.: Radiative forcing by long-lived greenhouse gases: Calculations with the AER radiative transfer models, J. Geophys. Res., 113(D13), D13103, doi:10.1029/2008JD009944, 2008.

https://doi.org/10.5194/acp-2019-1011
Preprint. Discussion started: 2 December 2019

Janjić, Z. I.: The Step-Mountain Eta Coordinate Model: Further Developments of the Convection, Viscous Sublayer, and Turbulence Closure Schemes, Mon. Weather Rev., 122(5), 927–945, doi:10.1175/1520-0493(1994)122<0927:TSMECM>2.0.CO;2, 1994.

Miao, Y. and Liu, S.: Linkages between aerosol pollution and planetary boundary layer structure in China, Sci. Total Environ., 650, 288–296, doi:10.1016/J.SCITOTENV.2018.09.032, 2019.

Miao, Y., Hu, X.-M., Liu, S., Qian, T., Xue, M., Zheng, Y. and Wang, S.: Seasonal variation of local atmospheric circulations and boundary layer structure in the Beijing-Tianjin-Hebei region and implications for air quality, J. Adv. Model. Earth Syst., 7(4), 1602–1626, doi:10.1002/2015MS000522, 2015.

Miao, Y., Liu, S., Zheng, Y. and Wang, S.: Modeling the feedback between aerosol and boundary layer processes: a case study in Beijing, China, Environ. Sci. Pollut. Res., 23(4), 3342–3357, doi:10.1007/s11356-015-5562-8, 2016.

Miao, Y., Guo, J., Liu, S., Liu, H., Li, Z., Zhang, W. and Zhai, P.: Classification of summertime synoptic patterns in Beijing and their associations with boundary layer structure affecting aerosol pollution, Atmos. Chem. Phys., 17(4), 3097–3110, doi:10.5194/acp-17-3097-2017, 2017a.

Miao, Y., Guo, J., Liu, S., Liu, H., Zhang, G., Yan, Y. and He, J.: Relay transport of aerosols to Beijing-Tianjin-Hebei region by multi-scale atmospheric circulations, Atmos. Environ., 165, 35–45, doi:10.1016/j.atmosenv.2017.06.032, 2017b.

Miao, Y., Liu, S., Guo, J., Huang, S., Yan, Y. and Lou, M.: Unraveling the relationships between boundary layer height and PM2.5 pollution in China based on four-year radiosonde measurements, Environ. Pollut., 243, 1186–1195, doi:10.1016/j.envpol.2018.09.070, 2018.

Miao, Y., Li, J., Miao, S., Che, H., Wang, Y., Zhang, X., Zhu, R. and Liu, S.: Interaction Between Planetary Boundary Layer and PM2.5 Pollution in Megacities in China: a Review, Curr. Pollut. Reports, doi:10.1007/s40726-019-00124-5, 2019a.

Miao, Y., Liu, S. and Huang, S.: Synoptic pattern and planetary boundary layer structure associated with aerosol pollution during winter in Beijing, China, Sci. Total Environ., 682, 464–474, doi:10.1016/j.scitotenv.2019.05.199, 2019b.

Nakanishi, M. and Niino, H.: An improved Mellor-Yamada Level-3 model: Its numerical stability and application to a regional prediction of advection fog, Boundary-Layer Meteorol., 119(2), 397–407, doi:10.1007/s10546-005-9030-8, 2006.

Nielsen-Gammon, J. W., Powell, C. L., Mahoney, M. J., Angevine, W. M., Senff, C., White, A., Berkowitz, C., Doran, C. and Knupp, K.: Multisensor estimation of mixing heights over a coastal city, J. Appl. Meteorol. Climatol., 47(1), 27–43, doi:10.1175/2007JAMC1503.1, 2008.

Oke, T. R.: Boundary Layer Climates, Routledge., 2002.

Philipp, A., Beck, C., Huth, R. and Jacobeit, J.: Development and comparison of circulation type classifications using the COST 733 dataset and software, Int. J. Climatol., doi:10.1002/joc.3920, 2014.

Quan, J., Gao, Y., Zhang, Q., Tie, X., Cao, J., Han, S., Meng, J., Chen, P. and Zhao, D.: Evolution of planetary boundary layer under different weather conditions, and its impact on aerosol concentrations, Particuology, 11(1), 34–40, doi:10.1016/j.partic.2012.04.005, 2013.

Seidel, D. J., Ao, C. O. and Li, K.: Estimating climatological planetary boundary layer heights from radiosonde observations: Comparison of methods and uncertainty analysis, J. Geophys. Res., 115(D16), D16113, doi:10.1029/2009JD013680, 2010.

Stefan, S., Necula, C., and Georgescu, F.: Analysis of long-range transport of particulate matters in connection with air circulation over Central and Eastern part of Europe, Phys. Chem. Earth, 35, 523–529, doi:10.1016/j.pce.2009.12.008, 2010.

Stull, R. B.: An Introduction to Boundary Layer Meteorology, edited by R. B. Stull, Springer Netherlands, Dordrecht., 1988.

Sun, T., Che, H., Qi, B., Wang, Y., Dong, Y., Xia, X., Wang, H., Gui, K., Zheng, Y., Zhao, H., Ma, Q., Du, R. and Zhang, X.: Characterization of vertical distribution and radiative forcing of ambient aerosol over the Yangtze River Delta during 2013–2015, Sci. Total Environ., 650, 1846–1857, doi:10.1016/j.scitotenv.2018.09.262, 2019.

Tie, X., Zhang, Q., He, H., Cao, J., Han, S., Gao, Y., Li, X. and Jia, X. C.: A budget analysis of the formation of haze in Beijing, Atmos. Environ., 100, 25–36, doi:10.1016/j.atmosenv.2014.10.038, 2015.

Wang, L., Wang, H., Liu, J., Gao, Z., Yang, Y., Zhang, X., Li, Y. and Huang, M.: Impacts of the near-surface urban boundary layer structure on PM2.5 concentrations in Beijing during winter, Sci. Total Environ., 669, 493–504, doi:10.1016/j.scitotenv.2019.03.097, 2019.

Wang, H., Peng, Y., Zhang, X., Liu, H., Zhang, M., Che, H., Cheng, Y. and Zheng, Y.: Contributions to the explosive growth of PM2.5 mass due to aerosol–radiation feedback and decrease in turbulent diffusion during a red alert heavy haze in Beijing–Tianjin–Hebei, China, Atmos. Chem. Phys., 18(23), 17717–17733, doi:10.5194/acp-18-17717-2018, 2018a.

Wang, X., Dickinson, R. E., Su, L., Zhou, C. and Wang, K.: PM 2.5 Pollution in China and How It Has Been Exacerbated by Terrain and Meteorological Conditions, Bull. Am. Meteorol. Soc., 99(1), 105–119, doi:10.1175/BAMS-D-16-0301.1, 2018b.

Ye, X., Song, Y., Cai, X. and Zhang, H.: Study on the synoptic flow patterns and boundary layer process of the severe haze events over the North China Plain in January 2013, Atmos. Environ., 124, 129–145, doi:10.1016/j.atmosenv.2015.06.011, 2016.

Zaveri, R. A.: A new lumped structure photochemical mechanism for large-scale applications, J. Geophys. Res. Atmos., doi:10.1029/1999JD900876, 1999.

Zaveri, R. A., Easter, R. C., Fast, J. D. and Peters, L. K.: Model for Simulating Aerosol Interactions and Chemistry (MOSAIC), J. Geophys. Res. Atmos., doi:10.1029/2007JD008782, 2008.

Zhang, J. P., Zhu, T., Zhang, Q. H., Li, C. C., Shu, H. L., Ying, Y., Dai, Z. P., Wang, X., Liu, X. Y., Liang, A. M., Shen, H. X. and Yi, B. Q.: The impact of circulation patterns on regional transport pathways and air quality over Beijing and its surroundings, Atmos. Chem. Phys., 12(11), 5031–5053, doi:10.5194/acp-12-5031-2012, 2012.

Zhang, R., Jing, J., Tao, J., Hsu, S.-C., Wang, G., Cao, J., Lee, C. S. L., Zhu, L., Chen, Z., Zhao, Y., and Shen, Z.: Chemical characterization and source apportionment of PM2:5 in Beijing: seasonal perspective, Atmos. Chem. Phys., 13, 7053–7074, doi:10.5194/acp-13-7053-2013, 2013.

Zhong, J., Zhang, X., Wang, Y., Sun, J., Zhang, Y., Wang, J., Tan, K., Shen, X., Che, H., Zhang, L., Zhang, Z., Qi, X., Zhao, H., Ren, S. and Li, Y.: Relative contributions of boundary-layer meteorological factors to the explosive growth of PM2.5

https://doi.org/10.5194/acp-2019-1011
Preprint. Discussion started: 2 December 2019

Atmospheric Chemistry and Physics Discussions

during the red-alert heavy pollution episodes in Beijing in December 2016, J. Meteorol. Res., 31(5), 809–819, doi:10.1007/s13351-017-7088-0, 2017.

Zhong, J., Zhang, X., Dong, Y., Wang, Y., Liu, C., Wang, J., Zhang, Y. and Che, H.: Feedback effects of boundary-layer meteorological factors on cumulative explosive growth of PM 2.5 during winter heavy pollution episodes in Beijing from 2013 to 2016, Atmos. Chem. Phys., doi:10.5194/acp-18-247-2018, 2018.

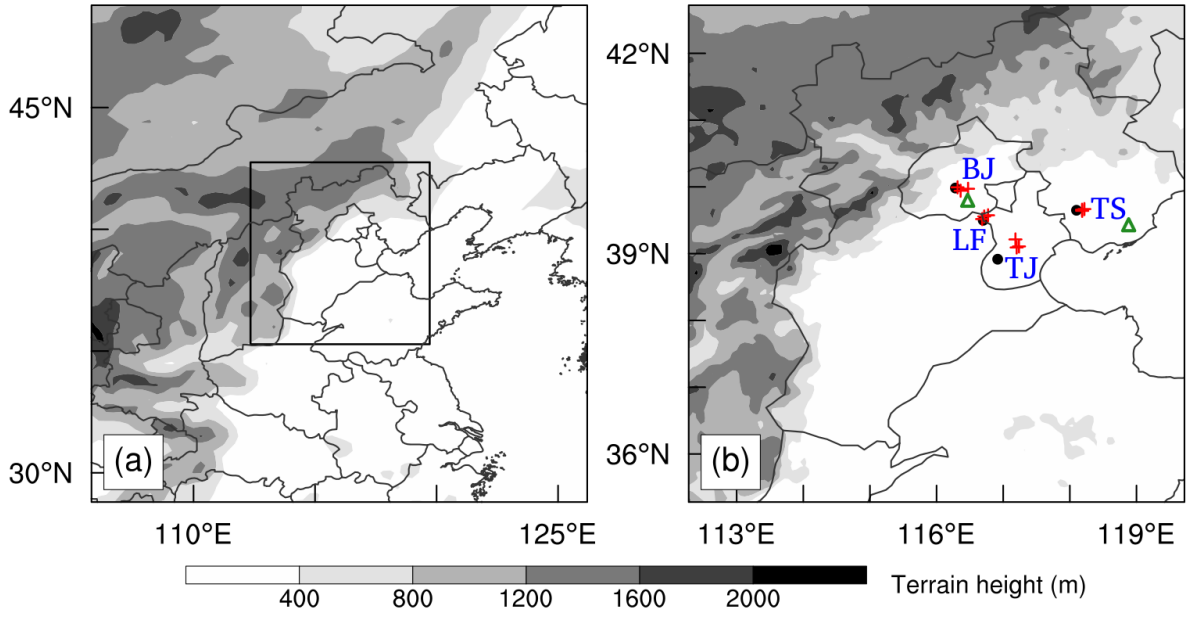

Figure 1: Maps of terrain height in (a) the outer domain and (b) the inner domain. In Fig. 1b, the locations of surface meteorological stations and air quality monitoring stations in Beijing (BJ), Langfang (LF), Tianjin (TJ) and Tangshan (TS) are marked by the black dots and the red crosses, respectively. The sounding sites are denoted by the green triangle.

https://doi.org/10.5194/acp-2019-1011
Preprint. Discussion started: 2 December 2019

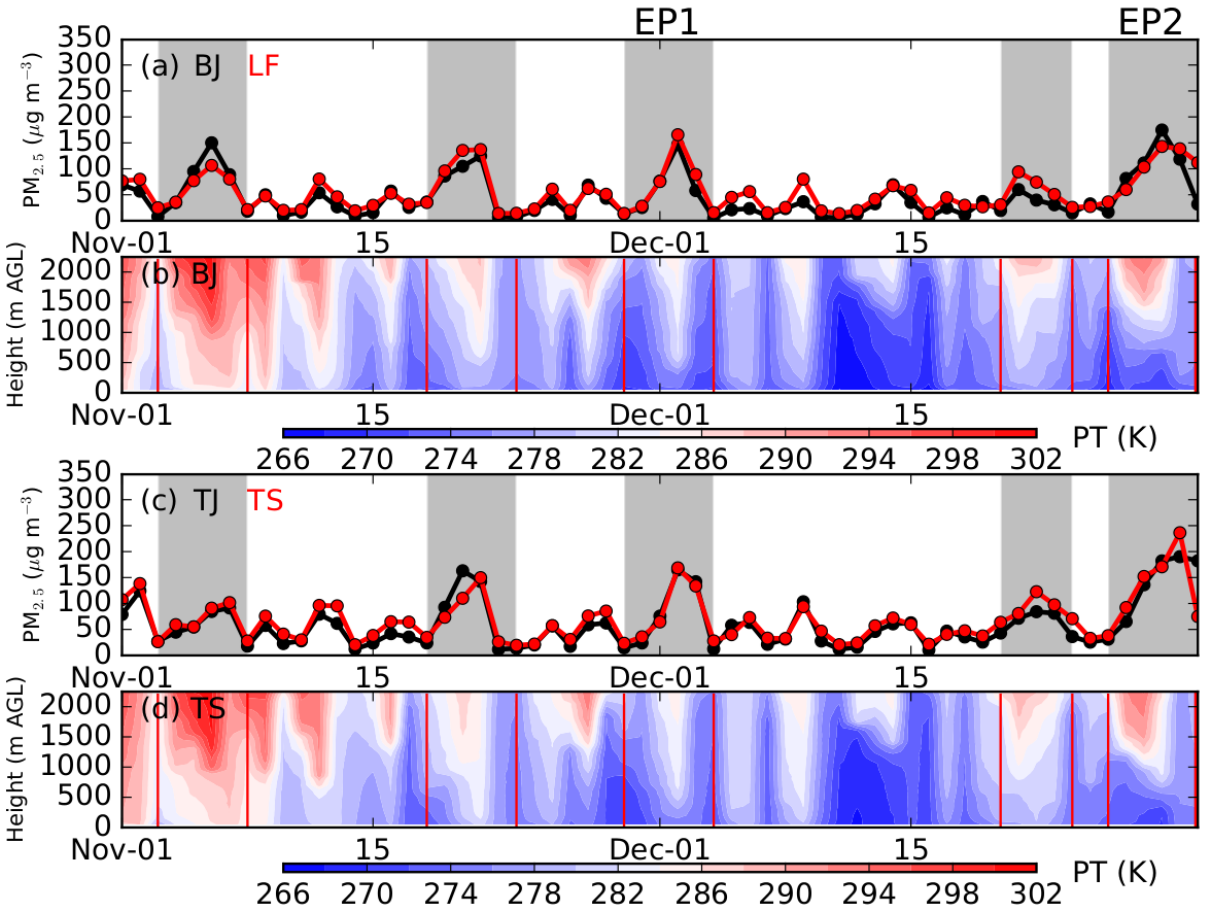

Figure 2: Time series of observed $PM_{2.5}$ concentration from 1 November to 31 December in 2017 in (a) Beijing and Langfang, (c) Tianjin and Tangshan. The vertical structure of potential temperature (PT) derived from the sounding data at 2000 BJT in (b) Beijing and (d) Tangshan. Five heavy pollution episodes associated with strong thermal inversions are marked by the grey shadings.

335

https://doi.org/10.5194/acp-2019-1011
Preprint. Discussion started: 2 December 2019

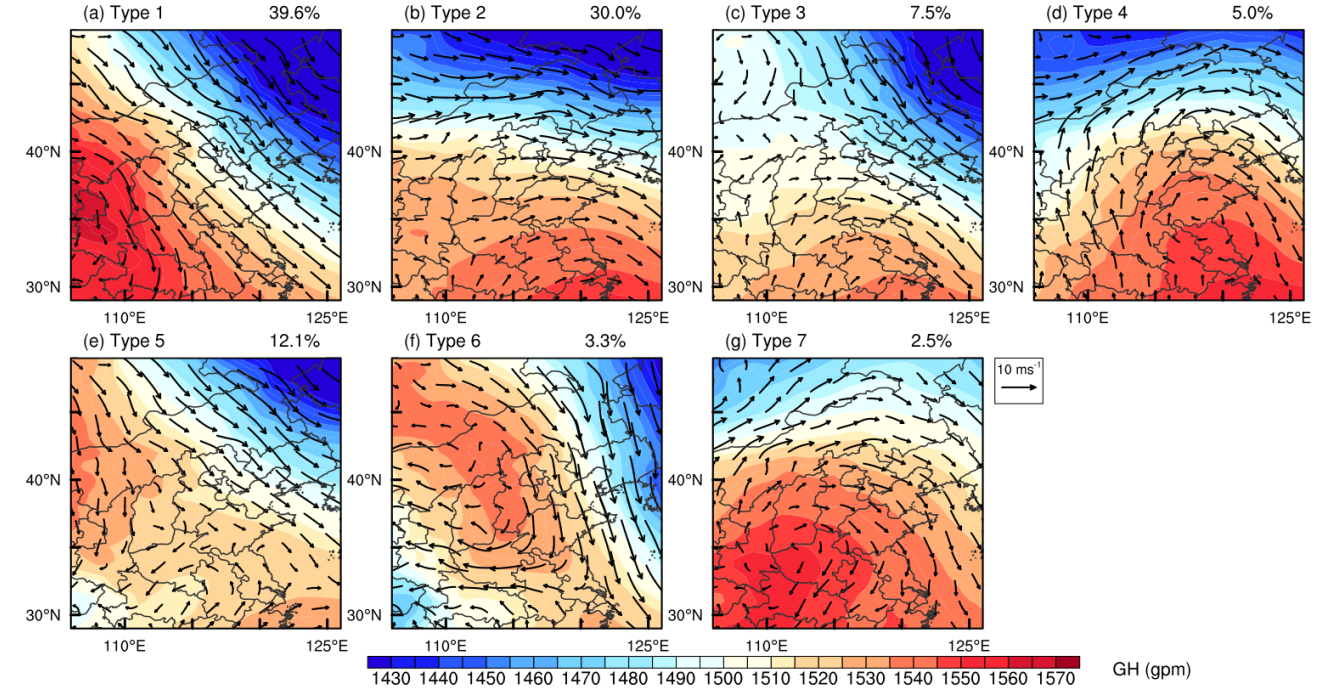

Figure 3: The 850-hPa geopotential height (GH) fields and wind vector fields for the seven classified patterns. The occurrence frequency of each synoptic pattern are also given.

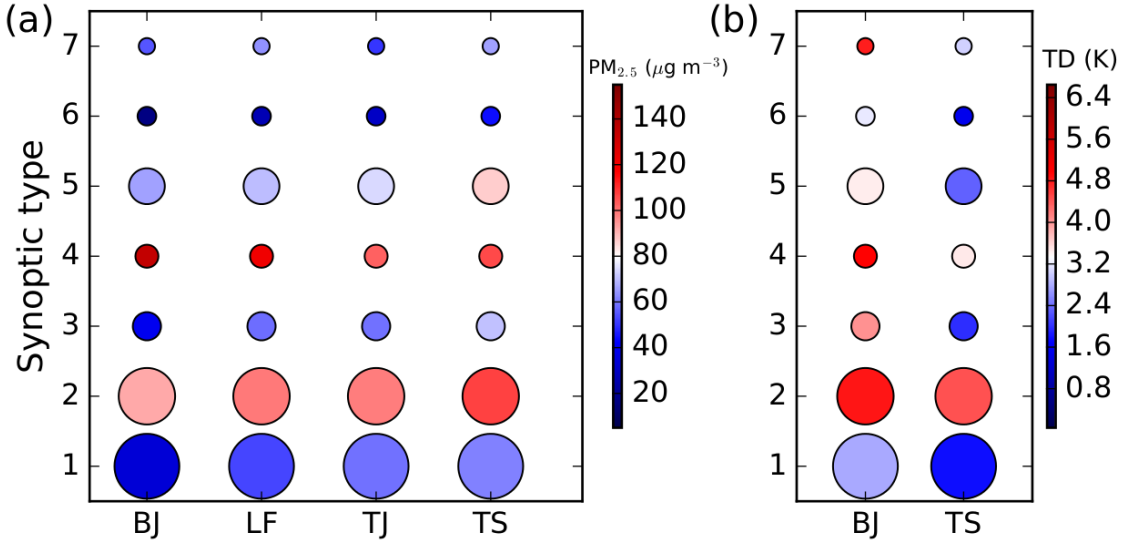

Figure 4: (a) Averaged $PM_{2.5}$ concentrations under different synoptic conditions in Beijing, Langfang, Tianjin and Tangshan, and (b) associated thermal differences (TD) of PT between 100 m and 1000 m AGL in Beijing and Tangshan. The TD equals PT at 1000-m minus PT at 100-m. The size of circle represents the occurrence frequency of each synoptic type.

https://doi.org/10.5194/acp-2019-1011
Preprint. Discussion started: 2 December 2019

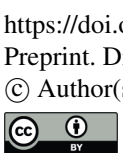

Atmospheric Chemistry and Physics Discussions

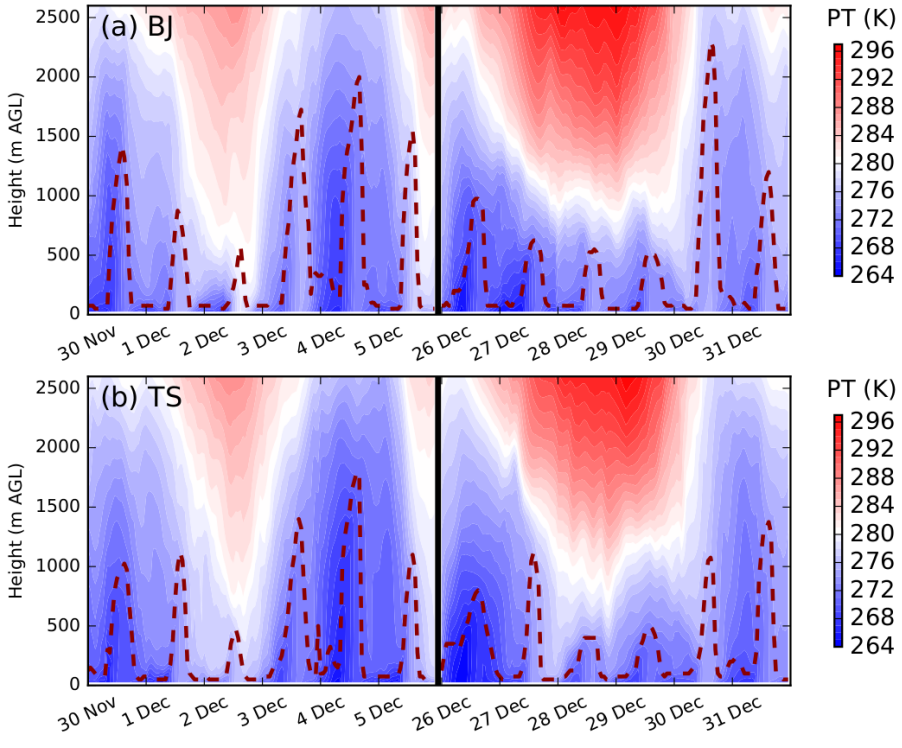

Figure 5: Vertical structure of simulated PT in (a) Beijing and (b) Tangshan during the EP1 (November 30 to December 5) and the EP2 (December 26 to 31). The PT profiles were derived from the BASE simulations of the grids nearest to the sounding sites. The boundary layer height (BLH) is denoted by the red dash line.

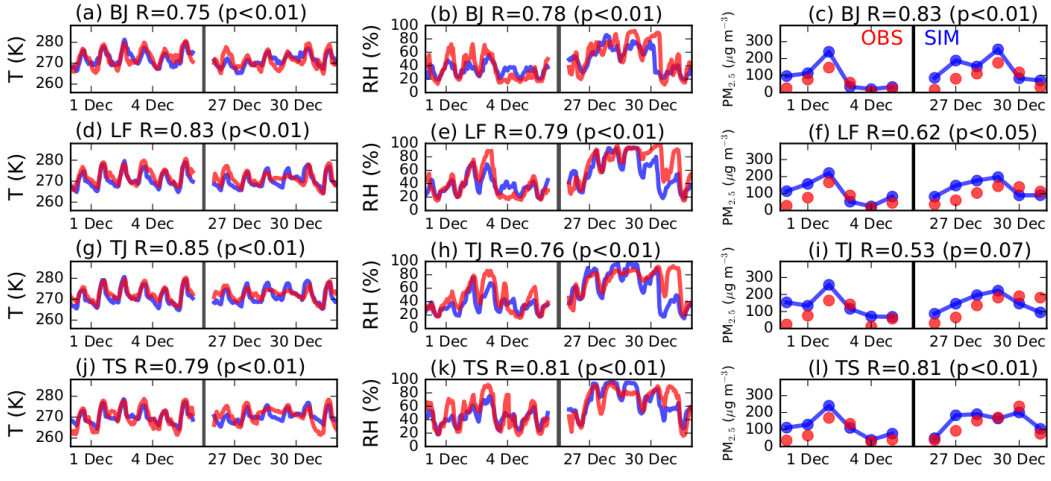

Figure 6: Time series of observed (in red) and simulated (in blue) 2-m temperature (T), 2-m relative humidity (RH), and $PM_{2.5}$ concentration in (top to bottom) Beijing, Langfang, Tianjin and Tangshan during the EP1 and EP2. The correlation coefficients (R) between the observations and simulations are also given for each panel.

https://doi.org/10.5194/acp-2019-1011
Preprint. Discussion started: 2 December 2019

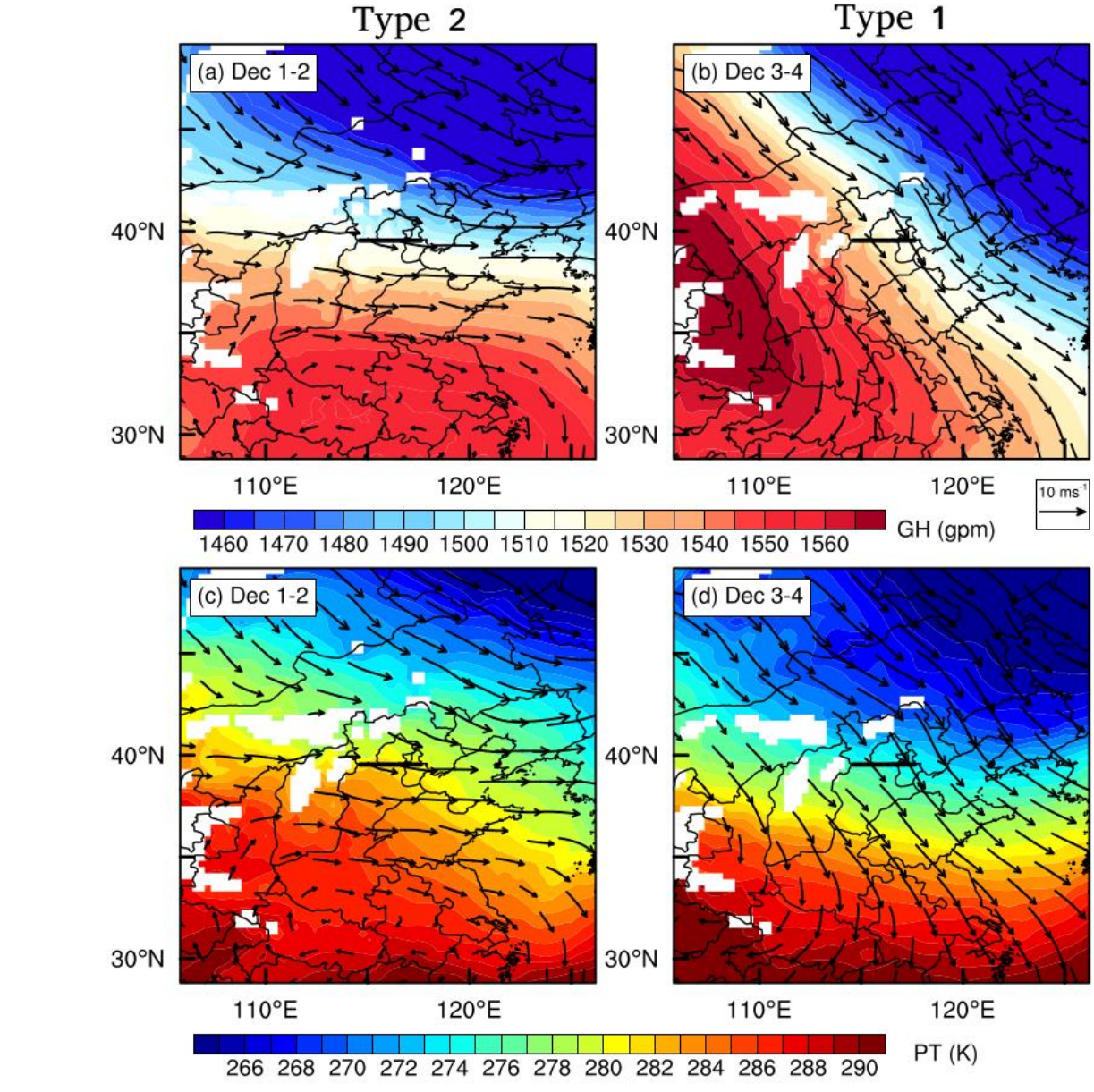

Figure 7: Averaged 850-hPa (a, b) GH and (c, d) PT fields during (left) December 1-2, and (right) December 3-4, overlaid with the wind vector fields. The black line across the BTH indicates the locations of cross section shown in Fig. 8.

https://doi.org/10.5194/acp-2019-1011
Preprint. Discussion started: 2 December 2019

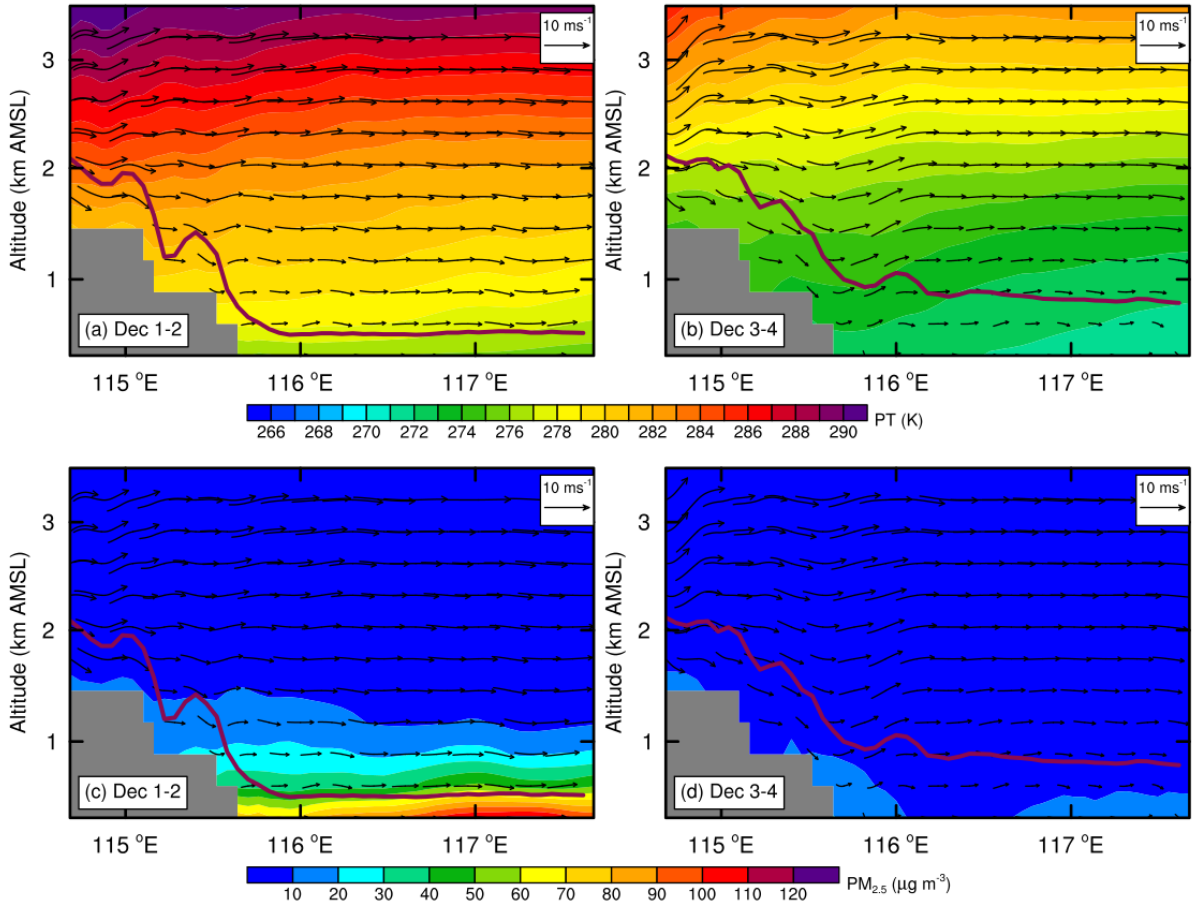

Figure 8: Vertical cross sections of simulated (a, b) PT, (c, d) $PM_{2.5}$ concentration during (left) December 1-2, and (right) December 3-4. The locations of cross section (~39.5 °N) are indicated by the black line in Fig. 7. The BLH is denoted by the red line for each panel. Note that the vertical velocity is multiplied by a factor of 10 when plotting the wind vectors.

https://doi.org/10.5194/acp-2019-1011
Preprint. Discussion started: 2 December 2019

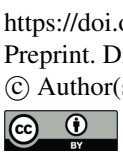

Atmospheric Chemistry and Physics Discussions

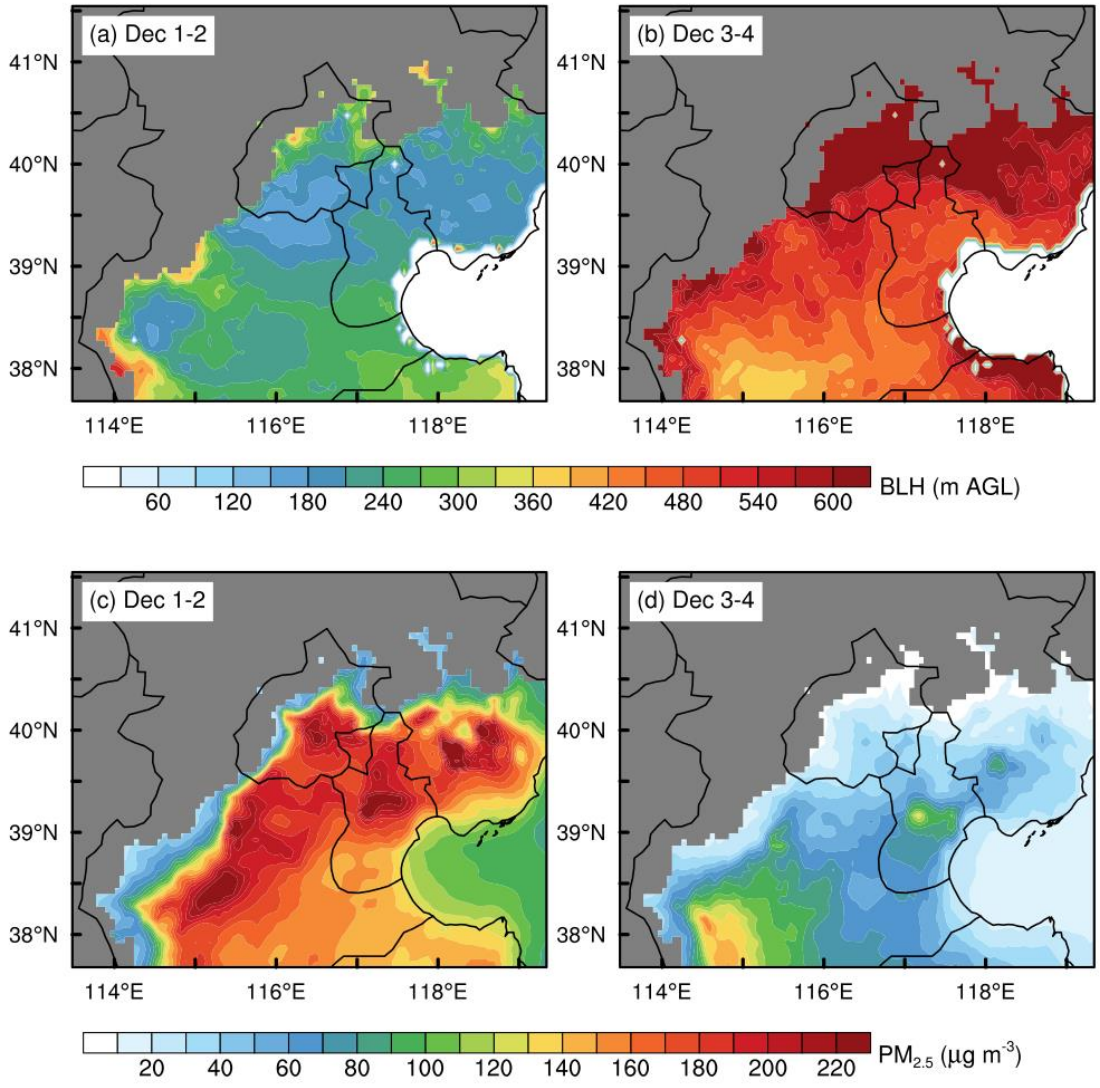

Figure 9: Spatial distribution of averaged (a, b) BLH and (c, d) $PM_{2.5}$ concentration during (left) December 1-2, and (right) December 3-4.

https://doi.org/10.5194/acp-2019-1011
Preprint. Discussion started: 2 December 2019

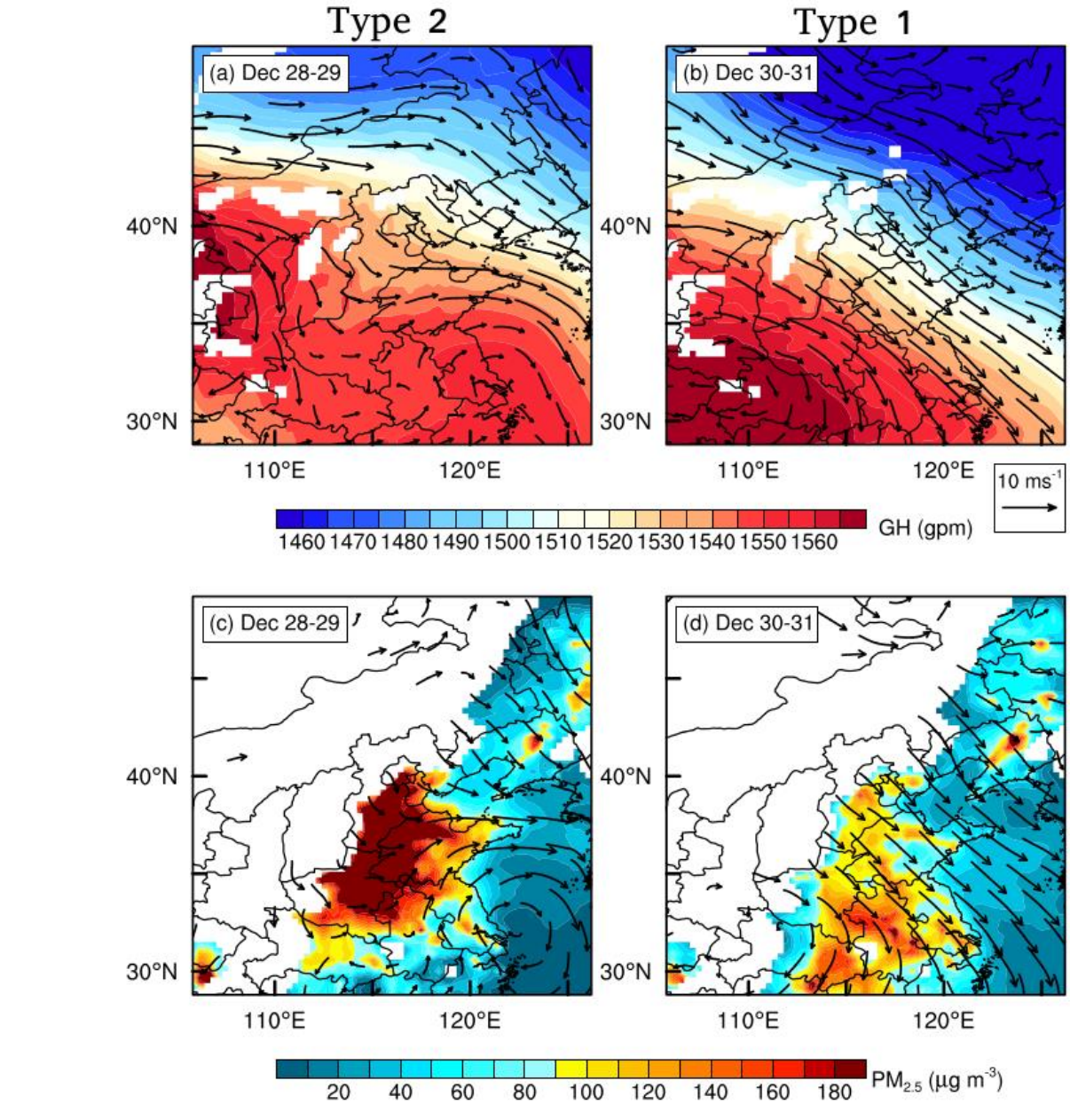

Figure 10: Simulated (top) 850-hPa GH and wind fields, and (bottom) near-surface $PM_{2.5}$ concentration overlaid with 900-hPa wind fields during December 28-31.

https://doi.org/10.5194/acp-2019-1011
Preprint. Discussion started: 2 December 2019

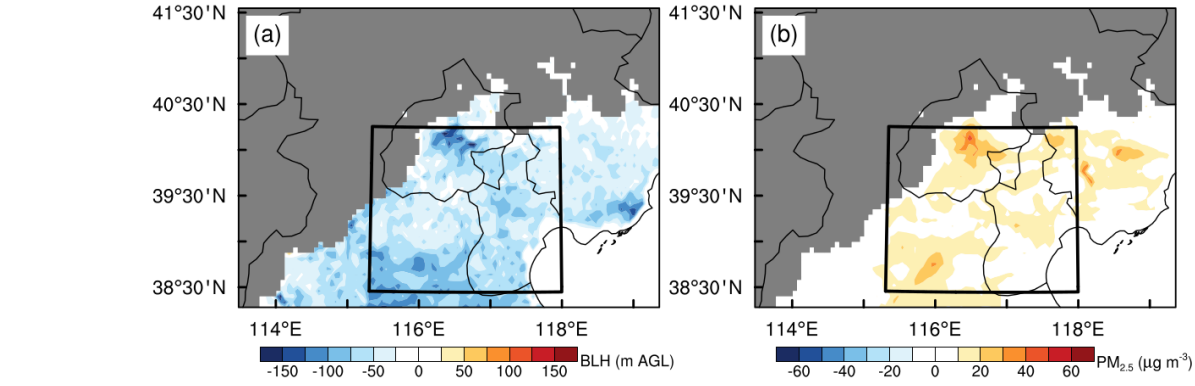

Figure 11: Perturbations induced by the aerosol radiative effect on (a) BLH and (b) near-surface $PM_{2.5}$ concentration during 0800 to 1800 BJT on December 1-2. The perturbations are estimated as the differences between the BASE and EXP simulations. The black square outlines the region of interest (ROI) for the vertical profiles of $PM_{2.5}$ and PT shown in Fig. 12.

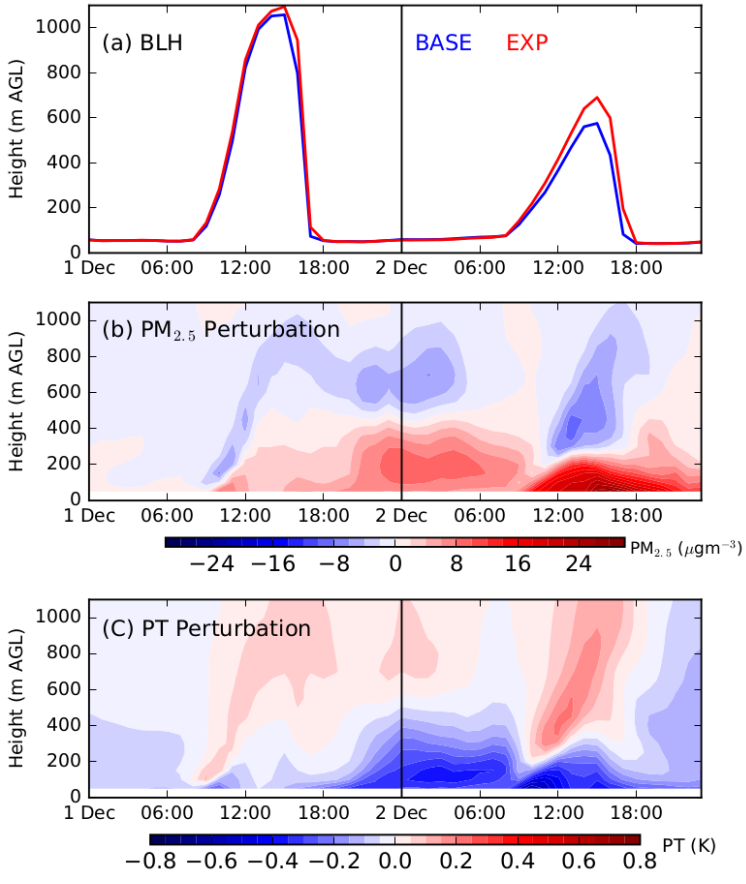

Figure 12: (a) Time series of BLH in the ROI on December 1-2, derived from the BASE (in blue) and EXP (in red) simulations. Perturbations induced by the aerosol radiative effect on the vertical profile of (b) $PM_{2.5}$ and (c) PT in the ROI.